Article published online: 2022-05-19

Original article

A 3D Monte Carlo Method for Estimation of Patient-specific Internal Organs Absorbed Dose for ^{99m}Tc-hynic-Tyr^3-octreotide Imaging

Mehdi Momennezhad, Shahrokh Nasseri[1], Seyed Rasoul Zakavi[2], Ali Asghar Parach[3], Mahdi Ghorbani, Ruhollah Ghahraman Asl

Department of Medical Physics, Faculty of Medicine, [1]Department of Medical Physics, Medical Physics Research Center, [2]Department of Nuclear Medicine, Nuclear Medicine Research Center, Mashhad University of Medical Sciences, Mashhad, [3]Department of Medical Physics, Shahid Sadoughi University of Medical Sciences, Yazd, Iran

Abstract

Single-photon emission computed tomography (SPECT)-based tracers are easily available and more widely used than positron emission tomography (PET)-based tracers, and SPECT imaging still remains the most prevalent nuclear medicine imaging modality worldwide. The aim of this study is to implement an image-based Monte Carlo method for patient-specific three-dimensional (3D) absorbed dose calculation in patients after injection of ^{99m}Tc-hydrazinonicotinamide (hynic)-Tyr^3-octreotide as a SPECT radiotracer. ^{99m}Tc patient-specific *S* values and the absorbed doses were calculated with GATE code for each source-target organ pair in four patients who were imaged for suspected neuroendocrine tumors. Each patient underwent multiple whole-body planar scans as well as SPECT imaging over a period of 1–24 h after intravenous injection of ^{99m}hynic-Tyr^3-octreotide. The patient-specific *S* values calculated by GATE Monte Carlo code and the corresponding *S* values obtained by MIRDOSE program differed within 4.3% on an average for self-irradiation, and differed within 69.6% on an average for cross-irradiation. However, the agreement between total organ doses calculated by GATE code and MIRDOSE program for all patients was reasonably well (percentage difference was about 4.6% on an average). Normal and tumor absorbed doses calculated with GATE were slightly higher than those calculated with MIRDOSE program. The average ratio of GATE absorbed doses to MIRDOSE was 1.07 ± 0.11 (ranging from 0.94 to 1.36). According to the results, it is proposed that when cross-organ irradiation is dominant, a comprehensive approach such as GATE Monte Carlo dosimetry be used since it provides more reliable dosimetric results.

Keywords: GATE Monte Carlo package, MIRDOSE, patient-specific dosimetry, *S* value

Introduction

Technetium-99m (^{99m}Tc)-hydrazinonicotinamide (hynic)-Tyr^3-octreotide as an alternative to Indium-111 (^{111}In)-diethylenetriaminepentaacetic acid (DTPA)-octreotide is a diagnostic radiotracer that is frequently used for localization of primary and metastatic sites of the neuroendocrine tumors (NETs).[1-4]

Access this article online

Quick Response Code:

Website: www.wjnm.org

DOI: 10.4103/1450-1147.174700

Gallium-68 (^{68}Ga)-labeled DOTA-conjugated octreotide is another diagnostic radiotracer for NETs that has been recently used by several groups,[5-7] but SPECT-based tracers are easily available and more widely used than PET-based tracers, and SPECT imaging still remains the most prevalent nuclear medicine imaging modality worldwide. Compared with ^{111}In-labeled somatostatin analog, the imaging by ^{99m}Tc-hynic-Tyr^3-octreotide is performed with low energy collimators and entails low cost and low radiation dose for the patient with better image quality, thus making it more attractive.[3,4] Also, the relatively low accumulation in nontarget tissues, rapid detection of somatostatin receptor-positive tumors, and reproducible radiolabeling procedures are some other favorable characteristics of ^{99m}Tc-hynic-Tyr^3-octreotide for imaging applications.[2,8-10] Therefore, accurate activity

Address for correspondence:
Dr. Ruhollah Ghahraman Asl, Department of Medical Physics, Faculty of Medicine, Mashhad University of Medical Sciences, Pardis –e Daneshgah, Vakil Abad Blvd., Mashhad, Iran. E-mail: ghahramanasl@gmail.com

quantification and organ dose estimations related to this diagnostic radiotracer by implementation of the Monte Carlo method in the form of patient personalized dosimetry are needed.

Several personal computational software based on standardized reference models [according to the International Commission on Radiological Protection (ICRP) or Medical Internal Radiation Dose (MIRD) committee models] have been proposed to assess the radiation absorbed dose in diagnostic and therapeutic contexts in nuclear medicine. Some of these software such as MIRDOSE program and another version (i.e. OLINDA/EXM program) are commercially available.[11-17] Using these programs, the mean absorbed dose imparted to the target tissue and the dose factors (i.e. *S* values) at the organ level can be acquired more easily according to the medical internal radiation dose (MIRD) approach for most of the radionuclides. The ability to adjust the reported doses for patient-specific organ masses is also provided with OLINDA/EXM program. However, these mean absorbed doses may be significantly influenced by nonuniform doses and a temporarily changing dose rate. Moreover, regarding the therapeutic radiopharmaceuticals, evidences indicate that deterministic biological effects including tumor response and normal tissue toxicity are not well-predicted by mean absorbed doses.[18] Furthermore, although the self-absorbed dose to the tumors could be obtained with unit density sphere models (i.e., nodule modules) in MIRDOSE or OLINDA/EXM programs; contributions to tumor dose from other organs and tissues cannot be included. This is an additional drawback for radionuclides with high energy photons or with significant nonnegligible gamma emissions.[19]

More accurate dosimetry can be obtained by performing a three-dimensional (3D) full image-based Monte Carlo simulation.[14,16] The patient-specific anatomy and radiopharmaceutical distribution on the basis of morphological and functional 3D images are considered in image-based Monte Carlo simulation.[19,20] In the radiation field, GATE Monte Carlo platform has attractive features[21] and its use for radionuclide dosimetry applications has been validated in several studies.[16,22-24] However, in our search in Medline, very few papers were noticed to have been published on the application of this popular code in the field of clinical diagnostic procedures.

In this study, the aim is to implement an image-based 3D Monte Carlo method based on the GATE Monte Carlo platform[25] for voxel-by-voxel absorbed dose calculation of internal organs in patients with histologically confirmed neuroendocrine tumor. The calculated results by GATE Monte Carlo method were compared with the data obtained with MIRDOSE 3.1 program (Oak Ridge Institute for Science and Education, Oak Ridge, TN 37831) as commercially available software for evaluation of the simulation method.

Materials and Methods

Radiopharmaceutical labeling

^{99m}Tc-hynic-Tyr^3-octreotide was constructed from a kit produced at Pars isotope company (PICo, Tehran, Iran). Radiolabeling was executed by dissolving 1 mL of 0.2 M phosphate buffer (pH 7.0) to the freeze-dried kit formulation then 1 mL of fresh ^{99m}Tc-pertechnetate containing up to 2 GBq was immediately added to the solution. The mixture was heated in a boiling water bath for 20–30 min.

Patient studies

Four patients comprising two males and two females with diagnosed or suspected neuroendocrine tumor who had been referred to the nuclear medicine department were selected. All the patients were approved by the Local Ethics Committee of Mashhad University of Medical Sciences. Each patient's demography, including mass of the organs were considered in this study is summarized in Table 1. MIRD phantom data are reported for comparison. ^{99m}Tc-hynic-Tyr^3-octreotide imaging was performed with a dual head gamma camera (E-Cam, Siemens Medical System Inc., USA) using a parallel hole, low-energy high-resolution (LEHR) collimator (Siemens Healthcare, Erlangen, Germany). A triple-energy window (TEW) method for scatter estimation, with a 15% window for photo-peak and 7% for both lower and upper scattering was used.[26-28] For each patient, four to five whole-body planar scans and a single SPECT scan were obtained over a period of 1–24 h after intravenous injection of 629–740 MBq of ^{99m}Tc-hynic-Tyr^3-octreotide. Whole body anterior and posterior views were recorded in a protocol of 256 × 1024 matrixes with a pixel size of 4.79 mm and a scan speed of 20 cm/min with an auto-contour mode. The SPECT scans were acquired over 360 (circular orbit) in 32 view/head and 20 s/frame and recorded in a 128 × 128 matrix. Computed tomography (CT) acquisition was performed before SPECT imaging by taking multiple slices in 512 × 512 matrices in helical mode, by using 25 mA current at 130 keV using a Siemens CT scanner (Siemens, ARTX, Munich, Germany). The CT images were used to create attenuation maps and for measurement of diameter of the patient's body. In some cases, CT images were used to determine the organ boundaries.

3D SPECT image reconstruction and activity quantification

The SPECT image reconstruction was performed using ordered subset expectation maximization (OSEM)

Table 1: Demographic data for the four patients and the two mathematic phantoms with the masses of the normal organs considered in this study

	Age (years)	Sex	Weight (kg)	Height (cm)	Organ mass (g)		
					Kidneys	Liver	Spleen
Patient 1	27	Male	61.0	164	220.3	1315.4	395.3
Patient 2	42	Male	84.0	179	308.6	2239.9	306.7
Patient 3	64	Female	73.0	155	266.1	1245.1	214.2
Patient 4	63	Female	53.0	158	280.4	1284.0	357.8
MIRD adult phantom*	-	Male	73.7	167	299.0	1910.0	183.0
MIRD adult phantom*	-	Female	56.8	157	275.0	1400.0	150.0

*Mirdose-Cristy-Eckerman-Stabin phantom

algorithm (with four subsets and eight iterations) on a clinical processing station using Syngo MI Applications 2012 (VA46C software, Siemens Healthcare, Forchheim, Germany). No postsmoothing and resolution recovery were applied to the reconstructed images. Isocontours were drawn with a 40% threshold in the reconstructed images and the count density in the tumors and normal organs of interest were calculated for all the patients by summing the counts within the target volume of interest (VOI). Scattering correction was performed using the triple energy window (TEW) method that has been used for ^{99m}Tc SPECT imaging before. An effective μ-value = 0.15 cm^{-1} was applied according to the MIRD pamphlet No. 16[28] for attenuation correction in each target VOI. The absolute activity in tumors and normal organs was calculated according to Equation 1 by correcting the counts within the target VOI and dividing by the calibration factor:

$$A(j) = \frac{R_0(j)}{K} = \frac{R_{Corr}(j)}{K.T}.f \qquad \text{Equation 1}$$

where $R_{Corr}(j)$ is the count rate corrected in the drawn VOIs and f is the self-absorption correction factor in the source organ ($f = [(\mu_j d_j/2)/\sinh(\mu_j d_j/2)]$) ($\mu_j$ and d_j are source region attenuation coefficient and source thickness, respectively). T is the transmission factor that can be determined using the diameter of the patient's body and linear absorption coefficient of water in the energy range of the radioisotope.[28,29] K is the calibration factor (in terms of counting rate per unit activity) that was determined using SPECT acquisition of a point source of known activity determined using CRC®-15R dose calibrator (Capintec, Inc., Ramsey, New Jersey, USA), placed in the air at about 15 cm from the surface of each of the two detectors. This method was validated on physical phantoms and was applied on *in vivo* patient data.

Calculation of time activity curves and effective half-lives for patient data

The procedure used in this was performed approximately in a similar manner as described in the study by Grims *et al*.[1] with only a mild difference. A hybrid planar/SPECT approach was implemented to plot and integrate time-activity curves. The first image from the series of whole-body scans of each patient was selected, and oversized regions were manually drawn around each tumor and organ with significant uptake that included the kidneys, liver, and spleen. In patients with liver metastasis, regions were drawn only around the whole liver, and the individual metastases were not included in this analysis. Regions of interest (ROIs) were automatically created by applying a threshold of 40% of the maximum pixel counts. The choice of a fixed 40% threshold was based on the fact that this value has been already commonly used in clinical practice.[30] These two-dimensional (2D) ROIs were then manually registered in the data from corresponding regions in the remaining whole-body scans at subsequent time points. For each ROI segmented, adjacent background regions were drawn in order to perform background subtraction.[28] After the background and TEW scattering correction in most cases, the corrected counts were plotted versus time. No attenuation correction was performed for the planar studies since the attenuation correction factor should remain constant at each time point. For each source region, a monoexponential fitting through the planar data was used to find the effective decay constant, λ_{eff}. The decay constants were used to determine the effective half-life in each source ROI using $T_{eff} = 0.693/\lambda_{eff}$. A marker was placed beside the table in one of the patients to verify the procedure and to confirm the physical half-life of ^{99m}Tc (6.02 h). In the next step, the cumulated activity ($\tilde{A}$) of each source region was determined from each scaled curve and the corresponding activity was acquired from the SPECT image (A_{SPECT}) at the time of the SPECT acquisition (t_{SPECT}); $\tilde{A} = A_{SPECT}[\exp(\lambda_{eff} t_{SPECT})/\lambda_{eff}]$. The ^{99m}Tc time-integrated activity coefficients (TIACs) (i.e. residence times)[31] that are needed for organ dose calculation were also computed by dividing the cumulated activities by the injected activity ($\tilde{A}/A_{inj}$) for each source region. The TIAC for the remainder of the body was determined by subtraction of the TIACs calculated for all the segmented organs from that of the whole body.

Absorbed dose calculations

Organ-level approach

This approach is acknowledged by the MIRD Committee of the Society of Nuclear Medicine for patient organ dose estimations[31] from residence times that were calculated

from the patient's scintigraphic images. The organ level is based on the precomputed *S* values ($Sr_T \leftarrow r_S$) from model phantoms. ($Sr_T \leftarrow r_S$) is the mean absorbed dose in the target organ (r_T), per decay of a considered radionuclide in the source organ (r_S). Then, the target organ absorbed dose was simply obtained from multiplication of the *S* value and the total number of disintegrations in the source organ (i.e., cumulated activity $\tilde{A}$). The MIRDOSE 3.1 program (Oak Ridge Institute for Science and Education, Oak Ridge, TN 37831) was used to calculate the organ-level mean absorbed dose for various organs of each patient (in mGy/MBq). Moreover, the absorbed dose per cumulative activity (i.e., the *S* value) could be acquired by MIRDOSE using standardized phantoms in terms of mGy/MBq-s. The contributions of self-dose and cross-dose from other segmented organs were included in the mean dose of each target organ. The nodule module in the MIRDOSE was used to calculate the absorbed doses to tumors. The self-absorbed *S* values for unit-density spheres of masses that ranged from 0.01 g to 6000 g were calculated for several radionuclides and could be acquired by the nodule module. The contribution of absorbed dose to tumor from photons in the rest of the body is typically ignored in MIRDOSE program.

Voxel-level approach

A developed GATE Monte Carlo platform was publicly released by the OpenGATE collaboration,[25] version 6.1 that is based on GEANT4.9.3 patch 0.1, was used to perform patient-specific internal dosimetry in voxel level. A set of SPECT/CT fused images of the patients with dimensions of 128 × 128 matrix and voxel spacing of 4.79 × 4.79 × 4.79 mm^3 was used in order to define the geometry, attenuation map, and spatial distribution of the radiotracer in the simulation. The image fusion was performed manually by Syngo MI applications ((Siemens Healthcare, Forchheim, Germany) under the physician's supervision. Patient-specific fused images were used as input in simulations since tumors are sometimes not visible in the CT images (especially in nondiagnostic low-dose CT systems). ^{99m}Tc spectrum was defined according to ICRP publication No. 107.[32] Compton scattering, photoelectric absorption, and Rayleigh scattering were considered in the photon tracking. An approximate total number of 10^8 histories were simulated for each patient. A personal computer with 3.5 GHz Intel (R) Core (TM) i7-4770K processor and 8.0 GB random access memory was used in the running step for Monte Carlo simulation. A statistical uncertainty below 5% was achieved in each voxel, including voxels from nonsource organs. Similar to the organ level approach, dose distributions calculated by GATE Monte Carlo simulation included self-doses as well as the cross-doses from all source organs. Only patients in whom entire organs such as kidneys, liver, and spleen were visible in a single SPECT field of view were considered. Meanwhile, a separate dose distribution in the all target regions was calculated for each source organ. Thus, a set of *S* values for each source and target organ pair could be determined.

Evaluation of the dose estimation procedures

The dose estimates acquired by the organ-level and the voxel-level (i.e., the Monte Carlo simulation) methods were evaluated by: (1) Comparing the organ-level *S* values obtained from each method, (2) comparing the total tumor and organ doses calculated by each method, and (3) investigating the difference in the right and left kidney doses from the GATE Monte Carlo simulation.

Comparison of model and patient-specific S values at the organ level

The values of *S* ($r_T \leftarrow r_S$) based on the standard phantoms used by MIRDOSE, $S_{MIRDOSE}$ ($r_T \leftarrow r_S$), were compared to the *S* values calculated by GATE Monte Carlo simulation, S_{GATE} ($r_T \leftarrow r_S$), using patient-specific fused images. The percentage difference between the two *S* values for each source and target region pair was found. The MIRDOSE *S* values were mass scaled using patient-specific organ masses ($m^{-2/3}$ for photon and self-irradiation, where m is the mass of the target organ).

$$\Delta S(r_T \leftarrow r_S) = \frac{(S_{GATE}(r_T \leftarrow r_S) - S_{MIRDOSE}(r_T \leftarrow r_S))}{S_{MIRDOSE}(r_T \leftarrow r_S)} \times 100 \qquad \text{Equation 2}$$

The average, standard deviation, and minimum and maximum percentage differences for entire organs of each patient and the entire patient population were calculated. In this work, the results obtained with MIRDOSE software were arbitrarily considered as the reference.

Total dose assessment

The mean tumor and normal organ absorbed doses that were calculated by GATE Monte Carlo code were compared to the tumor and organ doses calculated by MIRDOSE by finding the percentage differences between doses estimated by each of these two methods. The self- and cross-organ irradiation contributions were included in the comparison of tumor and normal organ doses. It should be noted that tumor doses calculated by MIRDOSE using the sphere model consider self-dose only. Finally, the 3D dose distributions calculated by GATE Monte Carlo method were compared visually by plotting the integrated dose volume histograms (DVHs) for tumor and normal organs of all patients.

Paired organ analysis

In order to investigate the potential shortcomings of the assumption that each of the paired organs receive an equal dose, we assessed the dose to the right and left kidneys separately from the GATE Monte Carlo calculation. The percentage difference between the right and left kidney doses (ΔK) was found using the following formula:

$$\Delta K = \frac{(D_{Left\ kidney} - D_{Right\ kidney})}{D_{Average\ kidneys}} \times 100 \qquad \text{Equation 3}$$

Results

Time activity curves and residence times

Tumors were revealed in three patients examined in this study. Samples of whole-body images from these patients are displayed in Figure 1. Patient characteristics, including age, sex, weight, height and organ masses that were considered in our study, are listed in Table 1. In spite of the height and weight for some patients being close to that of the MIRD phantom, the organ masses were different. Typical examples of organ time-activity curves for the left kidney, liver, and spleen for the four patients are shown in Figure 2. The median values for the effective and biological half-lifes, determined from the exponential fitting through the time-activity data for both tumors and organs are summarized in Table 2.

The residence times obtained from semi-quantification of SPECT images for the four patients are reported in Table 3. The mean absorbed dose values for each target organ were obtained at organ-level method when the residence times were interned in the software MIRDOSE. These residence times for patient-specific dose calculation were used in voxel-level method using GATE Monte Carlo method.

Comparison of organ-level S values

The results of the ^{99m}Tc S values obtained from MIRDOSE and GATE Monte Carlo methods in organ scale for the three organs (kidneys, liver, and spleen) are summarized in Table 4. Although the agreement in cross-irradiation S values was very poor (69.6% difference on an average), there was generally a good agreement for self-irradiation S values (4.3% difference on an average). The average $\Delta S\ (r_T \leftarrow r_S)$ values for the self-organ irradiation were -6.3, 3.8, and -0.5% for $S(spleen \leftarrow spleen)$, $(liver \leftarrow liver)$, and $S(kindneys \leftarrow kindneys)$, respectively. Similarly, for cross-organ irradiation the average $\Delta S(r_T \leftarrow r_S)$, values were -3.9 and 71.7% for S(kidneys←spleen) and S(liver←spleen), respectively. Additionally, the $\Delta S(r_T \leftarrow r_S)$ values and the ^{99m}Tc patient-specific S values calculated using GATE Monte Carlo code and the corresponding S values obtained by MIRDOSE (with self-target mass scaled) for each source-target organ pair are listed in Table 5.

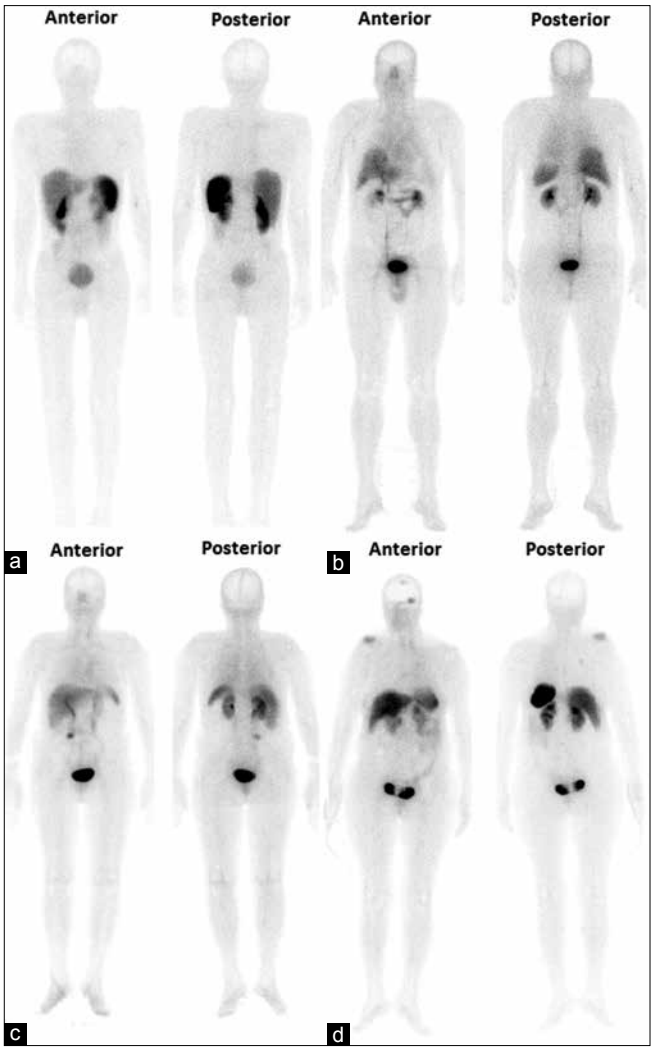

Figure 1: Anterior and posterior whole-body planar images at approximately 1–2 h after administration. (a): Neuroendocrine lesions is not revealed (patient1) (b) Neuroendocrine tumor is in multiple foci in the liver (patient 2) (c) Neuroendocrine tumor is in small bowel (right periumbilical region) (patient 3) (d) Neuroendocrine tumor is in the pancreatic head with metastasis to the right shoulder, left orbit and skull (patient 4)

Table 2: Effective and biologic half-lifes determined from monoexponential fitting through tumors and normal organs (data are median followed by range in parentheses)

Organ	Effective half-life (h)	Biologic half-life (h)
Kidneys	5.18 (4.76-5.85)	112.50 (23.73-209.69)
Liver	5.33 (4.95-5.41)	46.50 (27.85-53.79)
Spleen	5.87 (5.59-6.42)	136.25 (78.26-367.89)
Tumors	5.92 (5.87-5.97)	356.38 (235.58-784.19)
Whole body	4.72 (4.15-4.91)	25.79 (19.31-367.89)

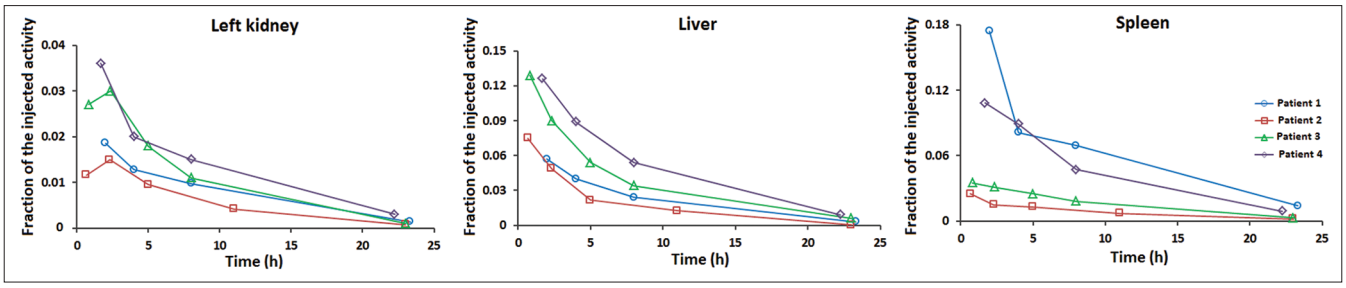

Figure 2: Decay time activity data for some of the normal organs of the four patients. The data were fitted with monoexponential function to find the effective decay constant

Total tumor and organ dose evaluation

The comparison of the absorbed doses obtained for tumor and three normal organs (kidneys, liver, and spleen) were restricted to whose geometry that was somewhat visible in planar/SPECT images. The absorbed doses calculated with GATE Monte Carlo simulation and MIRDOSE are presented as ratios with respect to GATE absorbed doses (GATE absorbed dose/MIRDOSE absorbed dose). In the vertical bar chart of Figure 3, the ratios between the GATE and MIRDOSE absorbed doses are reported for the four patients and the four regions considered. The histograms show that the spleen in patient 1, the liver in patient 2, and the tumor in patient 4 received slightly higher absorbed dose than the other organs. The average GATE/MIRDOSE ratio considered in all the organs was 1.07 ± 0.11, ranging from 0.94 to 1.36. Hence, the least agreement was found in the liver of patient 2 and similarly in the tumor of patient 4, where the percentage difference between the GATE Monte Carlo code and MIRDOSE doses was 24.3% and 35.5%, respectively. The average percentage difference for total tumor doses including self-dose and cross-dose contributions calculated by GATE and the tumor doses obtained from nodule module in MIRDOSE was 14.9% ±17.9%. This difference became -0.8% ±4.8% if the tumor's self-dose was calculated by GATE only and compared. Analysis of the self- and cross-organ irradiation data from GATE Monte Carlo simulation revealed that self-organ irradiation made approximately 77% higher contribution than cross-organ irradiations to the total dose calculated, on an average [Figure 4]. This is true for the majority of organs that are considered as sources and contain activity.

The estimated tumor masses and doses, along with the normal-organ doses for all patients with pathologic uptake are summarized in Table 6. In Figure 5, the integrated DVHs determined by the 3D GATE Monte Carlo method for each organ and tumor in each patient are illustrated separately. Analysis of these histograms clearly indicates the importance of patient-specific dosimetry and the large difference between the tumor and target organ doses in some cases in a diagnostic

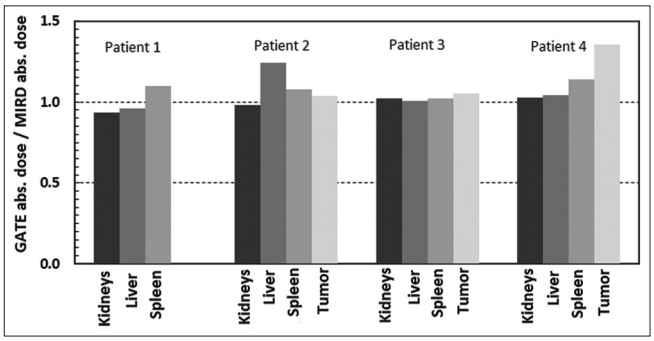

Figure 3: Ratio between GATE and MIRDOSE absorbed doses for the four patients. No tumor was visible in a single SPECT field of view for patient 1

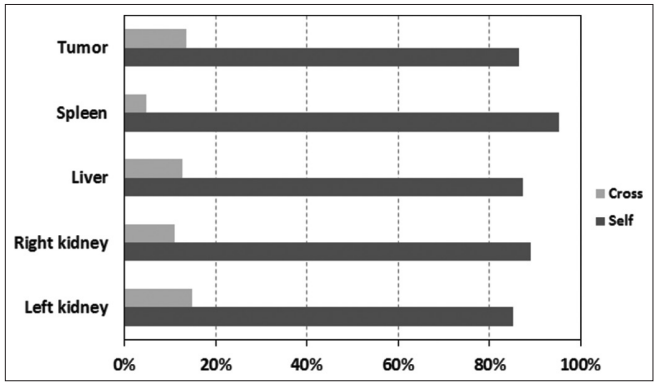

Figure 4: Average percent contributions of self- and cross-organ irradiation for all normal organ and tumor doses. The data were calculated by GATE Monte Carlo code

context. For example, the D_{90} (the minimum dose that at least covers 90% of the target volume) in the spleen is higher for patient 1 and patient 4 than the other organs of these patients. On the other hand, the DVHs calculated for the liver have lower values for some patients.

Dose comparison for the right and left kidneys

The comparison of ^{99m}Tc doses in both the kidneys, as calculated by GATE Monte Carlo method, is reported in Table 7. The average discrepancy between the doses deposited in the left and right kidneys of the four patients was 12.6%. This could be due to the differences in the

total activity uptake and the biological half-lives listed between the two kidneys.

Discussion

The purpose of this study was to implement the GATE Monte Carlo method for clinical patient-specific 3D dosimetry after injection of ^{99m}Tc-hynic-Tyr^3-octreotide.

Table 3: Residence times (h) for the source organs considered in this study

	Kidneys	Liver	Spleen	Tumor	Remainder
Patient 1	0.18	0.50	1.15	-	2.69
Patient2	0.13	0.32	0.20	0.04	3.30
Patient 3	0.24	0.80	0.38	0.14	3.80
Patient 4	0.25	1.15	1.18	0.03	3.47
Average±SD	0.20±0.06	0.69±0.36	0.73±0.51	0.07±0.06	3.32±0.47

Table 4: Summary of percentage differences ($\Delta S(r_T \leftarrow r_S)$) between the ^{99m}Tc patient-specific *S* values calculated using GATE Monte Carlo code and the corresponding *S* values used by MIRDOSE for each source and target region pair

Target	Source		
	Kidneys	Liver	Spleen
Kidneys	−0.5±2.2 (−2.0-2.7)	46.3±30.2 (1.1-65.2)	−3.9±21.3 (-28.9-21.4)
Liver	44.5±30.8 (−1.6-61.9)	3.8±1.4 (2.5-5.7)	71.7±42.7 (8.0-97.1)
Spleen	−2.7±22.3 (−28.6-24.3)	71.5±42.9 (8.0-98.0)	−6.3±12.3 (-15.9-11.9)

Data are mean±standard deviation; the range is provided in parentheses

Our study demonstrated that image-based dose calculation built on GATE Monte Carlo platform could provide reliable patient individualized dose estimates. Dose distributions calculated by GATE Monte Carlo simulation approximately took the maximum time of running for 2–3 h. The use of the variance reduction techniques and parallel computing platform[33] can substantially decrease the computation time.

To date, the hybrid planar/SPECT methods are widely used as acceptable approaches for 3D dosimetry[34] and this is fine as long as their limitations are understood. However, serial SPECT images are preferred but take a lot of time and hence, are not generally feasible.[34,35] Multiple planar whole-body scans and a single SPECT scan were used to obtain source region cumulative activities and residence times. The whole-body planar data were used only for determination of the effective decay constant in each source region in each patient. The accuracy of activity quantification has a large impact on patient-specific 3D dosimetry protocol.[36] Nonetheless, the physical phantom evaluation indicated that the accuracy of the activity quantification protocol was acceptable in the scale of human organs (i.e., greater than one centimeter) and the activity concentration range (>20 MBq). Discussion on all effects that degrade SPECT image quantification such as resolution recovery and the reconstruction algorithms are outside the scope of this work. We considered a uniform attenuation correction and uniform activity distribution in the source regions and used a TEW scattering correction technique.

Table 5: Percentage differences between ^{99m}Tc patient-specific *S* values calculated by GATE simulation and the corresponding reference *S* values (mGy/MBq-s) after scaling the target mass used by MIRDOSE for patients 1-4

Target	Method	Patient 1			Patient 2		
		Kidneys	Liver	Spleen	Kidneys	Liver	Spleen
Kidneys	$S_{GATE}(r_T \leftarrow r_S)$	1.73×10^{-5}	4.74×10^{-7}	8.21×10^{-7}	1.32×10^{-5}	2.88×10^{-7}	4.72×10^{-7}
	$S_{MIRDOSE}(r_T \leftarrow r_S)$	1.68×10^{-5}	2.93×10^{-7}	6.61×10^{-7}	1.34×10^{-5}	2.93×10^{-7}	6.61×10^{-7}
	$\Delta S(r_T \leftarrow r_S)$	2.7	61.9	24.3	−2.0	−1.6	−28.6
Liver	$S_{GATE}(r_T \leftarrow r_S)$	4.84×10^{-7}	4.38×10^{-6}	1.42×10^{-7}	2.96×10^{-7}	2.99×10^{-6}	1.31×10^{-7}
	$S_{MIRDOSE}(r_T \leftarrow r_S)$	2.93×10^{-7}	4.14×10^{-6}	7.20×10^{-8}	2.93×10^{-7}	2.90×10^{-6}	7.20×10^{-8}
	$\Delta S(r_T \leftarrow r_S)$	65.2	5.7	97.3	1.1	3.1	82.6
Spleen	$S_{GATE}(r_T \leftarrow r_S)$	8.02×10^{-7}	1.42×10^{-7}	1.17×10^{-5}	4.70×10^{-7}	1.34×10^{-7}	1.48×10^{-5}
	$S_{MIRDOSE}(r_T \leftarrow r_S)$	6.61×10^{-7}	7.20×10^{-8}	1.39×10^{-5}	6.61×10^{-7}	7.20×10^{-8}	1.65×10^{-5}
	$\Delta S(r_T \leftarrow r_S)$	21.4	97.1	−15.9	−28.9	86.4	−10.5
		Patient 3			**Patient 4**		
Kidneys	$S_{GATE}(r_T \leftarrow r_S)$	1.50×10^{-5}	5.54×10^{-7}	8.49×10^{-7}	1.44×10^{-5}	5.51×10^{-7}	7.35×10^{-7}
	$S_{MIRDOSE}(r_T \leftarrow r_S)$	1.52×10^{-5}	3.48×10^{-7}	8.18×10^{-7}	1.46×10^{-5}	3.48×10^{-7}	8.18×10^{-7}
	$\Delta S(r_T \leftarrow r_S)$	−1.3	59.3	3.8	−1.4	58.4	−10.2
Liver	$S_{GATE}(r_T \leftarrow r_S)$	5.54×10^{-7}	4.58×10^{-6}	1.18×10^{-7}	5.55×10^{-7}	4.54×10^{-6}	2.16×10^{-7}
	$S_{MIRDOSE}(r_T \leftarrow r_S)$	3.48×10^{-7}	4.47×10^{-6}	1.09×10^{-7}	3.48×10^{-7}	4.38×10^{-6}	1.09×10^{-7}
	$\Delta S(r_T \leftarrow r_S)$	59.2	2.5	8.0	59.5	3.8	98.0
Spleen	$S_{GATE}(r_T \leftarrow r_S)$	8.41×10^{-7}	1.18×10^{-7}	1.95×10^{-5}	7.28×10^{-7}	2.13×10^{-7}	1.30×10^{-5}
	$S_{MIRDOSE}(r_T \leftarrow r_S)$	8.18×10^{-7}	1.09×10^{-7}	2.18×10^{-5}	8.18×10^{-7}	1.09×10^{-7}	1.16×10^{-5}
	$\Delta S(r_T \leftarrow r_S)$	2.9	8.0	−10.5	−11.0	95.3	11.9

$\Delta S(r_T \leftarrow r_S) = 100 \times (S_{GATE}(r_T \leftarrow r_S) - S_{MIRDOSE}(r_T \leftarrow r_S))/S_{MIRDOSE}(r_T \leftarrow r_S)$

Table 6: Tumor mass, tumor doses, and normal organ doses for patients with pathologic uptake

	Tumor numbered	Tumor mass (g)	Dose (mGy/MBq)			
			Tumors	Kidneys	Liver	Spleen
Patient 1	-	-	-	0.016	0.009	0.049
Patient 2	2	47.54*	0.021‡	0.007	0.004	0.011
Patient 3	1	24.45	0.067	0.016	0.014	0.028
Patient 4	1	18.08	0.022	0.019	0.020	0.057
Mean±SD			0.037±0.027	0.014±0.005	0.012±0.007	0.036±0.021

*Total mass is listed for this case, ‡Average dose is listed for this case

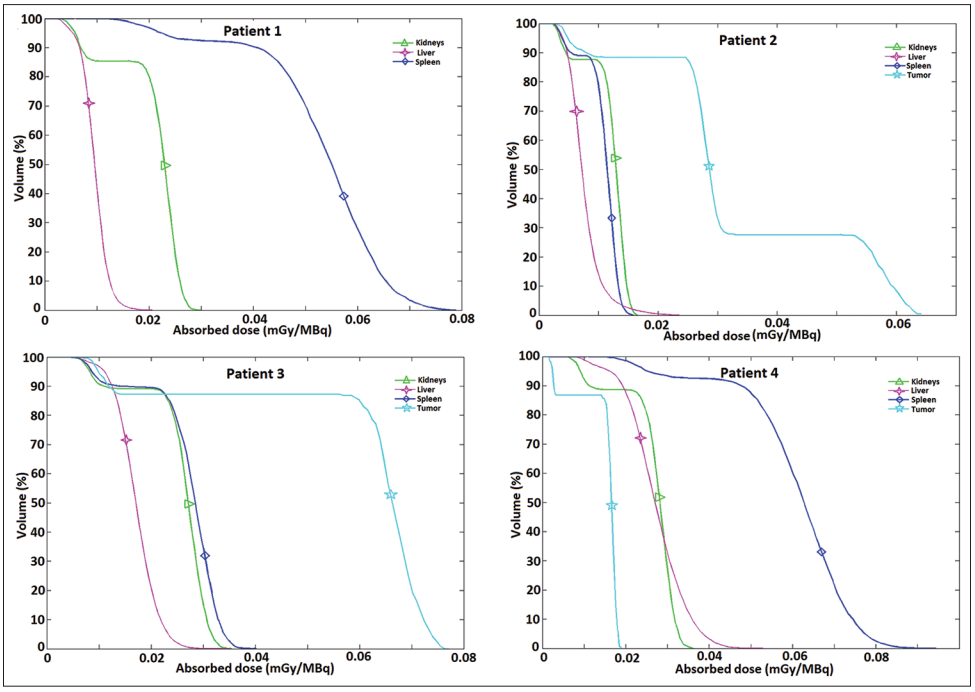

Figure 5: Integrated dose volume histograms based on 3D dose distributions calculated with GATE Monte Carlo code for regions and tumors considered in this study for each patient separately. From these DVHs, based on the large interpatient dose variation in normal organs and tumors, the importance of patient-specific dosimetry can be considered

A close agreement was observed based on comparison of the total organ doses calculated using GATE Monte Carlo code and MIRDOSE program [Figure 3] despite the large discrepancy in cross *S* values [Table 4]. This was related to the fact that the self-irradiation is the dominant contribution to the total dose per unit of cumulated activity [Figure 4]. Percentage differences in cross-organ *S* values acquired using GATE and MIRDOSE methods range from -28.9% to 98%. These results are concordant with other studies. Grimes and Celler[35] reported a range of -38% to 105% for ^{99m}Tc *S* values calculated from electron gamma shower (EGS) Monte Carlo code and OLINDA/EXM. Divoli *et al.*[37] reported a range of -51% to 84% between OLINDA/EXM and MCNPX Monte Carlo code for iodine-131 (^{131}I) *S* values. It can be concluded from this comparison that the MIRDOSE program is an acceptable tool for calculation of mean absorbed doses using standard models in the case of diagnostic radiopharmaceuticals such as ^{99m}Tc-hynic-Tyr^3-octreotide. It is reported for therapeutic radiopharmaceuticals such as ^{131}I and lutetium-177 (^{177}Lu) that have higher energy photons (364 keV and 208 keV, respectively), MIRDOSE is not accurate tool for patient-specific dosimetry[38] since the contributions of cross-irradiation are more significant. Gamma ray energy and radiation intensity are two factors that affect cross-organ contribution.[35] Analysis of the tumor doses calculated by GATE Monte Carlo code demonstrated that the nodule module in MIRDOSE program underestimates the total tumor dose by 14.9%, on an average. This is because the cross-dose contribution is included in GATE Monte Carlo code but not included in MIRDOSE. This difference is higher than that previously reported by Grimes and Celler (i.e. -8.8%).[35] They investigated tumors that ranged from 23 mL to 95 mL in volume; in the present study, tumors with a volume range of 18–47.5 mL were evaluated.

As listed in Table 6, the mean normal organ absorbed doses calculated by GATE Monte Carlo code in this work were 0.014 mGy/MBq, 0.012 mGy/MBq, and 0.036 mGy/MBq

Table 7: Percentage difference between right and left kidney doses (Δ*K*) calculated by Monte Carlo code with the corresponding biological half-life for each patient

	Δ*K*	T_{Biol} (h)	
	^{99m}Tc	Left kidney	Right kidney
Patient 1	11.9	178.9	240.5
Patient 2	9.1	38.8	16.2
Patient 3	14.7	29.2	18.3
Patient 4	14.6	356.4	38.7
Mean±SD	12.6±2.7	150.8±153.2	78.4±108.5

Δ*K*=100 × (left kidney dose-right kidney dose)/average kidney dose. SD: Standard deviation

for the kidneys, liver, and spleen, respectively. In a similar study with ^{99m}Tc-hynic-tektrotyd (TOC) imaging,[1] the reported doses for the kidneys, liver, and spleen were 0.021 mGy/MBq, 0.012 mGy/MBq, and 0.030 mGy/MBq, respectively. The doses estimated in the two studies agree within the provided uncertainties but they are significantly lower than the doses reported from ^{111}In-DTPA-octreotide imaging (0.41 mGy/MBq, 0.57 mGy/MBq, and 0.10 mGy/MBq for the kidneys, liver, and spleen, respectively).[39] The effective doses after ^{99m}Tc-hynic-Tyr^3-octreotide injection ranged from 0.007 mSv/MBq to 0.011 mSv/MBq. This range is approximately five to eight times lesser than the standard effective doses after ^{111}In-DTPA-octreotide injection (i.e., 0.054 mSv/MBq).[40] Nevertheless, lower radiation dose is desirable for patients undergoing repeated ^{99m}Tc-hynic-Tyr^3-octreotide scanning as well as for younger patients.

In Figure 5, the dose volume histograms for each target region determined using GATE Monte Carlo method for each patient are presented. These determinations were due to the voxel nature of the calculations. The definition of DVH for tumor and normal organs is crucial for prediction of the probability of tumor control as well as the unwanted effects of radiations on the proximity nontarget tissue, especially for radionuclide therapy. However, nuclear physicians may utilize the DVHs and the isodose curves obtained for optimization in radionuclide therapy plan. It is also evident from Table 7 that the doses to the left and right kidneys differed by up to 14.7%, for example, for patient 3. This discrepancy may be more serious in the therapeutic scenarios of paired organs when standard model dose estimation software is used.

Conclusions

This work provided a realistic GATE Monte Carlo simulation based on hybrid planar/SPECT imaging to provide better patient-specific 3D dose distribution than standard model internal dosimetry in a diagnostic context. The voxelized dose information could also be obtained easily from the GATE Monte Carlo simulation since there is a major limitation in organ-level dose estimation methods. Although the organ absorbed doses from ^{99m}Tc-hynic-Tyr^3-octreotide are usually low, patient-specific dosimetry built on imaging may be desirable for patients with repeated scanning or younger patients to estimate the stochastic biological effects (e.g., cancer induction) and also for pretherapy imaging dosimetry of patients who are candidates for a radionuclide therapy. Using a pretherapy tracer study, such dosimetric calculations might be more useful in an optimized treatment by radiopharmaceuticals and in ensuring the high safety and efficacy of the treatment. It is proposed that when cross-organ irradiation is dominant, a comprehensive approach such as GATE Monte Carlo dosimetry be used since it provides more reliable dosimetric results.

Acknowledgement

We express our gratitude to the all staff members of the Nuclear Medicine Department of Ghaem Hospital of Mashhad University of Medical Sciences for their sincere cooperation. This work was financially supported by Mashhad University of Medical Sciences with funding number 920325.

References

1. Grimes J, Celler A, Birkenfeld B, Shcherbinin S, Listewnik MH, Piwowarska-Bilska H, *et al*. Patient-specific radiation dosimetry of ^{99m}Tc-HYNIC-Tyr^3-octreotide in neuroendocrine tumors. J Nucl Med 2011;52:1474-81.
2. Decristoforo C, Mather SJ, Cholewinski W, Donnemiller E, Riccabona G, Moncayo R. ^{99m}Tc-EDDA/HYNIC-TOC: A new ^{99m}Tc-labelled radiopharmaceutical for imaging somatostatin receptor-positive tumours; first clinical results and intra-patient comparison with ^{111}In-labelled octreotide derivatives. Eur J Nucl Med 2000;27:1318-25.
3. Plachcinska A, Mikolajczak R, Maecke HR, Mlodkowska E, Kunert-Radek J, Michalski A, *et al*. Clinical usefulness of ^{99m}Tc-EDDA/HYNIC-TOC scintigraphy in oncological diagnostics: A preliminary communication. Eur J Nucl Med Mol Imaging 2003;30:1402-6.
4. Shinto AS, Kamaleshwaran KK, Mallia M, Korde A, Samuel G, Banerjee S, *et al*. Utility of ^{99m}Tc-Hynic-TOC in ^{131}I whole-body scan negative thyroid cancer patients with elevated serum thyroglobulin levels. World J Nucl Med 2015;14:101-8.
5. Putzer D, Kroiss A, Waitz D, Gabriel M, Traub-Weidinger T, Uprimny C, *et al*. Somatostatin receptor PET in neuroendocrine tumours: ^{68}Ga-DOTA0, Tyr^3-octreotide versus ^{68}Ga-DOTA0-lanreotide. Eur J Nucl Med Mol Imaging 2013;40:364-72.
6. Herrmann K, Czernin J, Wolin EM, Gupta P, Barrio M, Gutierrez A, *et al*. Impact of ^{68}Ga-DOTATATE PET/CT on the management of neuroendocrine tumors: The referring physician's perspective. J Nucl Med 2015;56:70-5.
7. Frilling A, Sotiropoulos GC, Radtke A, Malago M, Bockisch A, Kuehl H, *et al*. The impact of ^{68}Ga-DOTATOC positron emission tomography/computed tomography on the multimodal

management of patients with neuroendocrine tumors. Ann Surg 2010;252:850-6.

8. Gabriel M, Decristoforo C, Donnemiller E, Ulmer H, Watfah Rychlinski C, Mather SJ, *et al*. An intrapatient comparison of ^{99m}Tc-EDDA/HYNIC-TOC with ^{111}In-DTPA-octreotide for diagnosis of somatostatin receptor-expressing tumors. J Nucl Med 2003;44:708-16.
9. Korde A, Mallia M, Shinto A, Sarma HD, Samuel G, Banerjee S. Improved kit formulation for preparation of ^{99m}Tc-HYNIC-TOC: Results of preliminary clinical evaluation in imaging patients with neuroendocrine tumors. Cancer Biother Radiopharm 2014;29:387-94.
10. Koçyiğit Deveci E, Ocak M, Bozkurt MF, Türker S, Kabasakal L4, Uğur O. The diagnostic efficiency of ^{99m}Tc-EDDA/HYNIC-Octreotate SPECT-CT in comparison with ^{111}In-Pentetrotide in the detection of neuroendocrine tumours. Mol Imaging Radionucl Ther 2013;22:76-84.
11. Stabin MG. MIRDOSE: Personal computer software for internal dose assessment in nuclear medicine. J Nucl Med 1996;37:538-46.
12. Stabin MG, Sparks RB, Crowe E. OLINDA/EXM: The second-generation personal computer software for internal dose assessment in nuclear medicine. J Nucl Med 2005;46:1023-7.
13. Hobbs RF, Wahl RL, Lodge MA, Javadi MS, Cho SY, Chien DT, *et al*. ^{124}I PET-based 3D-RD dosimetry for a pediatric thyroid cancer patient: Real-time treatment planning and methodologic comparison. J Nucl Med 2009;50:1844-7.
14. Kost SD, Dewaraja YK, Abramson RG, Stabin MG. VIDA: A voxel-based dosimetry method for targeted radionuclide therapy using Geant 4. Cancer Biother Radiopharm 2015;30:16-26.
15. Grassi E, Fioroni F, Ferri V, Mezzenga E, Sarti MA, Paulus T, *et al*. Quantitative comparison between the commercial software STRATOS® by Philips and a homemade software for voxel-dosimetry in radiopeptide therapy. Phys Med 2015;31:72-9.
16. Marcatili S, Villoing D, Mauxion T, McParland BJ, Bardies M. Model-based versus specific dosimetry in diagnostic context: Comparison of three dosimetric approaches. Med Phys 2015;42:1288-96.
17. Sempau J, Wilderman SJ, Bielajew AF. DPM, a fast, accurate Monte Carlo code optimized for photon and electron radiotherapy treatment planning dose calculations. Phys Med Biol 2000;45:2263-91.
18. O'Donoghue JA. Implications of nonuniform tumor doses for radioimmunotherapy. J Nucl Med 1999;40:1337-41.
19. Ljungberg M, Sjogreen-Gleisner K. The accuracy of absorbed dose estimates in tumours determined by quantitative SPECT: A Monte Carlo study. Acta Oncol 2011;50:981-9.
20. Wilderman SJ, Dewaraja YK. Method for fast CT/SPECT-Based 3D Monte Carlo absorbed dose computations in internal emitter therapy. IEEE Trans Nucl Sci 2007;54:146-51.
21. Sarrut D, Bardies M, Boussion N, Freud N, Jan S, Letang JM, *et al*. A review of the use and potential of the GATE Monte Carlo simulation code for radiation therapy and dosimetry applications. Med Phys 2014;41:064301.
22. Parach AA, Rajabi H, Askari MA. Assessment of MIRD data for internal dosimetry using the GATE Monte Carlo code. Radiat Environ Biophys 2011;50:441-50.
23. Papadimitroulas P, Loudos G, Nikiforidis GC, Kagadis GC. A dose point kernel database using GATE Monte Carlo simulation toolkit for nuclear medicine applications: Comparison with other Monte Carlo codes. Med Phys 2012;39:5238-47.
24. Parach AA, Rajabi H, Askari MA. Paired organs-should they be treated jointly or separately in internal dosimetry? Med Phys 2011;38:5509-21.
25. The Open Gate Collaboration [updated 2014 Dec 5]. Available from: http://www.opengatecollaboration.org. [Last accessed on 2015 Jan 10].
26. Ichihara T, Ogawa K, Motomura N, Kubo A, Hashimoto S. Compton scatter compensation using the triple-energy window method for single- and dual-isotope SPECT. J Nucl Med 1993;34:2216-21.
27. Zeintl J, Vija AH, Yahil A, Hornegger J, Kuwert T. Quantitative accuracy of clinical ^{99m}Tc SPECT/CT using ordered-subset expectation maximization with 3-dimensional resolution recovery, attenuation, and scatter correction. J Nucl Med 2010;51:921-8.
28. Siegel JA, Thomas SR, Stubbs JB, Stabin MG, Hays MT, Koral KF, *et al*. MIRD pamphlet no. 16: Techniques for quantitative radiopharmaceutical biodistribution data acquisition and analysis for use in human radiation dose estimates. J Nucl Med 1999;40:37-61S.
29. Lyra M, Lagopati N, Charalambatou P, Vamvakas I. Patient-specific dosimetry in radionuclide therapy. Radiat Prot Dosimetry 2011;147:258-63.
30. Erdi YE, Wessels BW, Loew MH, Erdi AK. Threshold estimation in single photon emission computed tomography and planar imaging for clinical radioimmunotherapy. Cancer Res 1995;55(Suppl):5823-6s.
31. Bolch WE, Eckerman KF, Sgouros G, Thomas SR. MIRD pamphlet No. 21: A generalized schema for radiopharmaceutical dosimetry-standardization of nomenclature. J Nucl Med 2009;50:477-84.
32. Eckerman K, Endo A. ICRP Publication 107. Nuclear decay data for dosimetric calculations. Ann ICRP 2008;38:7-96.
33. OpenGATE-Collaboration. User's guide (Version 6.2) [updated 2012 Apr 9]. Available from: http://www.opengatecollaboration.org/UsersGuide. [Last accessed on 2015 Jan 10].
34. Dewaraja YK, Frey EC, Sgouros G, Brill AB, Roberson P, Zanzonico PB, *et al*. MIRD pamphlet No. 23: Quantitative SPECT for patient-specific 3-dimensional dosimetry in internal radionuclide therapy. J Nucl Med 2012;53:1310-25.
35. Grimes J, Celler A. Comparison of internal dose estimates obtained using organ-level, voxel S value, and Monte Carlo techniques. Med Phys 2014;41:092501-11.
36. Dewaraja YK, Wilderman SJ, Ljungberg M, Koral KF, Zasadny K, Kaminiski MS. Accurate dosimetry in ^{131}I radionuclide therapy using patient-specific, 3-dimensional methods for SPECT reconstruction and absorbed dose calculation. J Nucl Med 2005;46:840-9.
37. Divoli A, Chiavassa S, Ferrer L, Barbet J, Flux GD, Bardiès M. Effect of patient morphology on dosimetric calculations for internal irradiation as assessed by comparisons of Monte Carlo versus conventional methodologies. J Nucl Med 2009;50:316-23.
38. Loke KS, Padhy AK, Ng DC, Goh AS, Divgi C. Dosimetric considerations in radioimmunotherapy and systemic radionuclide therapies: A review. World J Nucl Med 2011;10:122-38.
39. ICRP. Radiation dose to patients from radiopharmaceuticals: (Addendum to ICRP Publication 53): ICRP Publication 80. Ann ICRP 1998;28:1-126.
40. Stabin MG. Internal dosimetry in nuclear medicine. Braz J Rad Sci 2013;1:1-15.

How to cite this article: Momennezhad M, Nasseri S, Zakavi SR, Parach AA, Ghorbani M, Asl RG. A 3D Monte Carlo method for estimation of patient-specific internal organs absorbed dose for ^{99m}Tc-hynic-Tyr^3-octreotide imaging. World J Nucl Med 2016;15:114-23.

Source of Support: Office of the vice president for research affairs in Mashhad University of Medical Sciences, Iran. **Conflict of Interest:** None declared.